BOLLETTINO DI GEOFISICA TEORICA ED APPLICATA VOL. 42, N. 3-4, PP. 281-304; SEP.-DEC. 2001

Analysis of dense array noise measurements using the modified spatial auto-correlation method (SPAC): application to the Grenoble area

B. BETTIG[1], P.Y. BARD[1,2], F. SCHERBAUM[3], J. RIEPL[4], F. COTTON[4], C. CORNOU[1] and D. HATZFELD[1]

[1] *Laboratoire de Géophysique Interne et Tectonophysique, Observatoire de Grenoble, Université Joseph Fourier, France*
[2] *Laboratoire Central des Ponts et Chaussées, Paris, France*
[3] *Institut für Geowissenschaften, Potsdam, Germany*
[4] *Institut de Protection et de Sûreté Nucléaire, Fontenay aux Roses, France*

(Received September 5, 2001; accepted November 22, 2001)

Abstract - Recent earthquakes outlined the importance of amplification effects in deep sedimentary basins where many large cities like Mexico City are located. This paper presents an application of the "modified spatial auto-correlation method" based on ambient vibrations analysis in order to obtain a model of the underlying local structure (velocity profiles for compressional and shear waves). We first describe the spatial auto-correlation method itself designed for regular, circular arrays. Then an improvement is presented that allows the use of irregular, almost arbitrarily shaped arrays. We then apply this technique to data obtained at two sites during a temporary experiment in Grenoble (March 99). Grenoble is an interesting site because of large, broad band amplification effects and very thick late quaternary deposits. The results compare relatively well with existing geophysical information from gravimetric, seismic reflection and borehole data. The relevance of the method for urban areas is therefore emphasized, considering its low cost and relative simplicity, and its performance for very thick deposits. However, some further theoretical and experimental investigations are required to clearly assess the capabilities and limitations of the method.

Corresponding author: P.-Y. Bard; Laboratoire de Géophysique Interne et Tectonophysique, Observatoire de Grenoble Université Joseph Fourier, BP 53, 38041 Grenoble Cedex 9, France; phone: +33 476828061; fax: +33 476828101; e-mail: pierre-yves.bard@obs.ujf-grenoble.fr

1. Introduction

We are interested here in the characterization of seismic hazard for big cities built on sedimentary basins, Grenoble being a typical case of large site amplification of seismic motion.

The nature of the filling (sediments) and its geometry induce vertical and horizontal reverberations of seismic waves because of the great impedance contrast with the bedrock at the interface. The trapping of surface waves generated by diffraction at the edges of the valley results in a particularly strong amplification of the seismic motion inside the basin.

One key point in estimating local site effects is the knowledge of basin structure: geometry of the interface between the filling and the bedrock, nature and thickness of the sediments. In the area of Grenoble, the knowledge of the basin geometry and filling was significantly improved recently: seismic reflection data (Dietrich et al., 2001), deep borehole, gravimetric studies (Vallon, 1999). This was a good reason to test a modified version of the spatial autocorrelation (SPAC) method with the ambient vibration measurements performed during a specific experiment (Scherbaum et al., 1999).

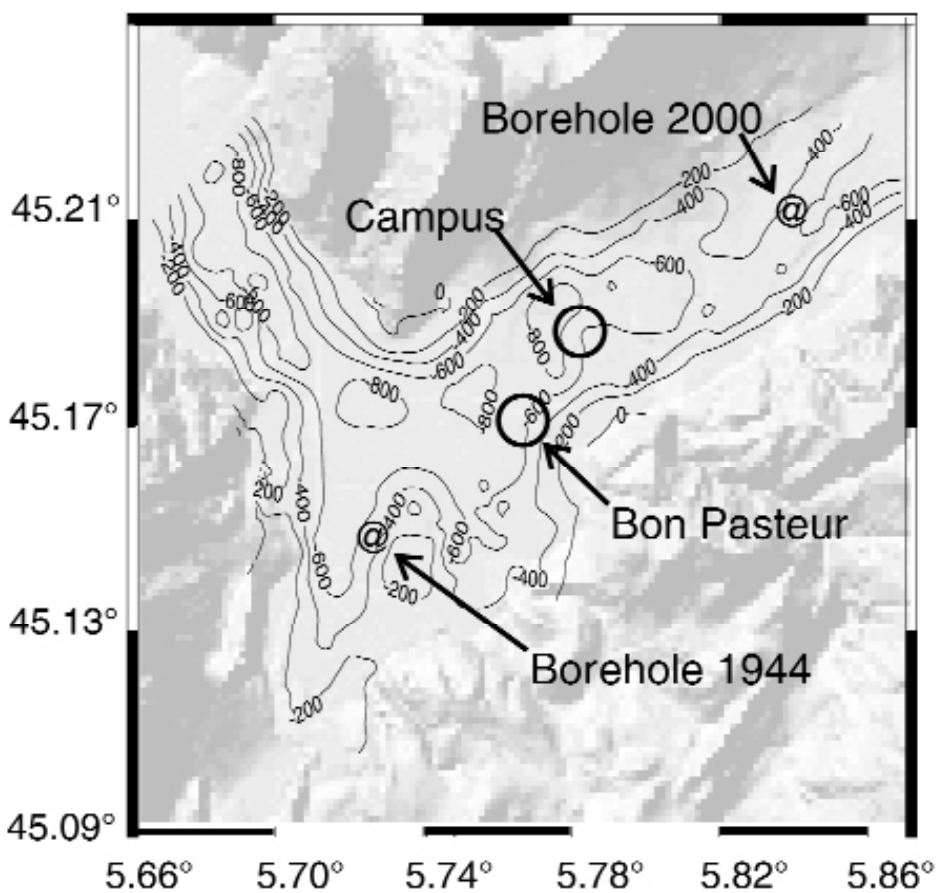

Fig. 1 - Digital elevation model of the Grenoble basin and 3D contour map of the depth of the basement (black lines; Vallon, 1999). Symbol @ show the locations of deep boreholes, and circles show sites Campus and Bon Pasteur (dense array background noise measurements).

The SPAC method was first designed by Aki (1957) to reveal the nature of the background seismic noise and also the characteristics of the propagation medium. We brought changes to Aki's original method in order to make it operational for urban investigations. Moreover, we tested this modified SPAC method to estimate its performance and the relevance of the improvements. The results presented, for the two sites “Campus” and “Bon Pasteur” (Fig. 1), show that even in thick sites, ambient vibration array measurements constitute a promising tool for deep investigations and contribute very significantly to seismic hazard assessment.

2. Temporary experiment at Grenoble site

2.1. The Grenoble site

Grenoble (Western Alps) location is characterized by a deep quaternary sediment-filled basin and the occurence of nearby moderate earthquakes. The city thus faces a non negligible seismic risk (Cotton et al., 1998): moderate seismicity, with strong amplification effects. The fundamental frequency of the basin is around [0.25-0.3Hz], and the amplification reaches values between 10 and 20 over a very wide frequency range [0.3-5Hz] (Lebrun, 1997). Very similar conditions may be found in most large alpine valleys. Using geological, geotechnical, seismic and gravity measurements, a 3D model of the Grenoble area was constructed. Bouguer anomaly analysis of gravity measurements at several hundred locations (Vallon, 1999) provided the underground bedrock's topography. This information is supported and calibrated by two deep boreholes made near Grenoble (Fig. 1).

The first was drilled more than fifty years ago (in 1943) in the southern part of the city. Although 400 meters deep, it did not reach the basement; two main formations, however, were identified from the rough logging (from 0 to 72 m depth, a coarse glacial material; from 72 to 400 m, lacustrine deposits) (Gignoux, 1944). The second was performed in 1999 to calibrate gravimetric and seismic data, in Montbonnot 10 km NE from the town center. It reached the basement at a 535 m depth (Cornou, 2002). As this measured bedrock depth agrees very well with the previous estimations based on gravimetric data, we may very reliably deduce that the maximum sediment thickness, which corresponds roughly to the crossing of the 3 valleys, is around 900 m.

This borehole and the seismic reflection surveys also brought many more details about the geotechnical structure of the quaternary deposits, including quantitative data on their density and velocities. The P-wave profile was accurately and consistently measured with sonic and down–hole devices, and was shown to increase with almost a linear gradient from 1400 m/sec at the very surface to 2100 m/s at 500 m depth. The average S-wave velocity over this thickness has also been directly measured (around 550 m/s), while its value at the surface lies around 250 m/s: one may therefore reasonably assume a linear gradient similar to the P-wave gradient, from 250 m/s at the surface, to 950 m/s at 500 m depth.

2.2. Grenoble 1999 experimentation

Between March 18 and April 1, 1999, a dense array experiment, to measure the ambient seismic noise in the Grenoble basin, was successfully conducted through a collaboration between the IPSN (Institut de Protection et de Sûreté Nucléaire) and the universities of Potsdam and Grenoble (Scherbaum et al., 999). The recording instruments of Postdam University (13 5s-3-components-Lennartz Le3D sensors, connected to 13 MarsLite stations with very precise GPS timing) were disposed in dense array at a total of 8 sites. At each site, the measurements lasted for at least 3 hours.

Since the arrays were originally designed for a semblance-based frequency wavenumber analysis, their shape was not adapted to Aki's SPAC method (see below). Therefore, we complemented the theoretical investigations in order to enlarge the application domain of the method to non-circular arrays (most current case of urban measurements). Fig. 2 shows the location and shape of both campus arrays (one of large aperture: 1.2 km, and one with high

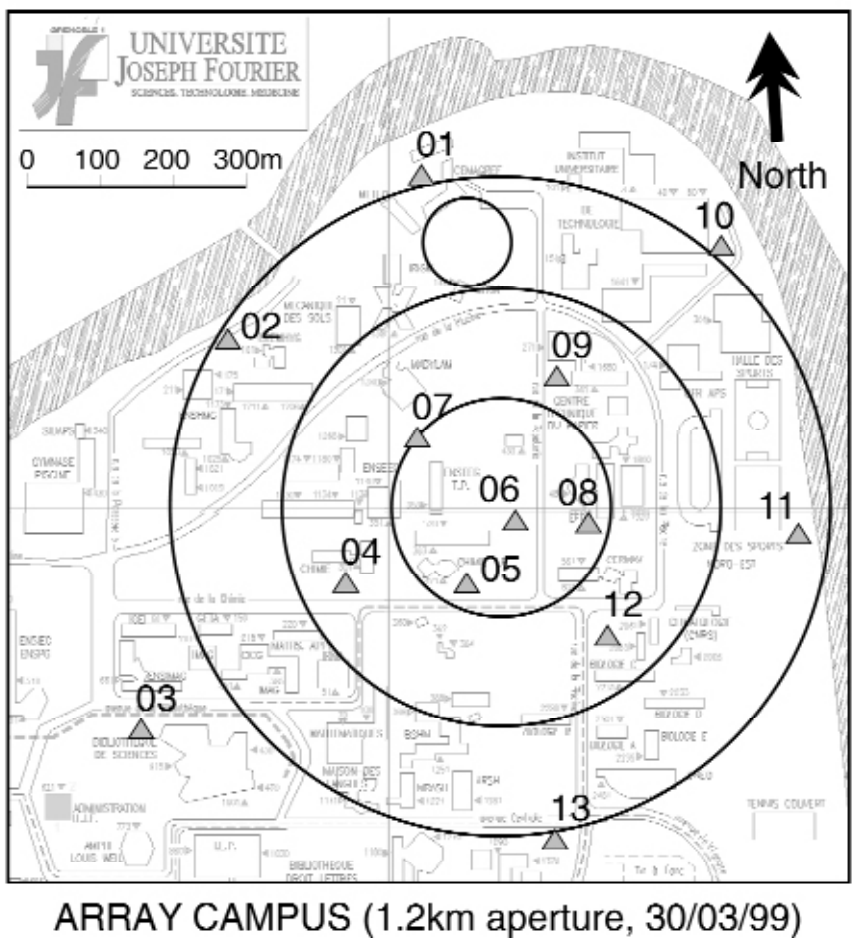

Fig. 2 - Map of the Campus of Grenoble University. The triangles show the location of the stations (large array). Stations should have been located around three circles, but buildings and other obstacles prevented us from installing a perfect in shape array. The small circle in the upper part of the figure corresponds to the small array location.

density: 20 m between neighbouring stations). If the smaller one can be considered as perfect in shape (stations located on three concentric circles), it is not the case for the large one (see also Fig. 3a). The original objective was to install the stations on three concentric circles, but buildings and obstacles of all sorts forced us to find other locations. The distribution of spacings and azimuths of all station pairs is thus very far from being regular, which prevents us from using the classical Aki SPAC formulation (see Fig. 3b).

3. The modified spatial auto-correlation (SPAC) method

The SPAC method is designed to estimate the dispersion curves for surface waves by analysing the correlation between noise recordings made at nearby sites. From these curves, we

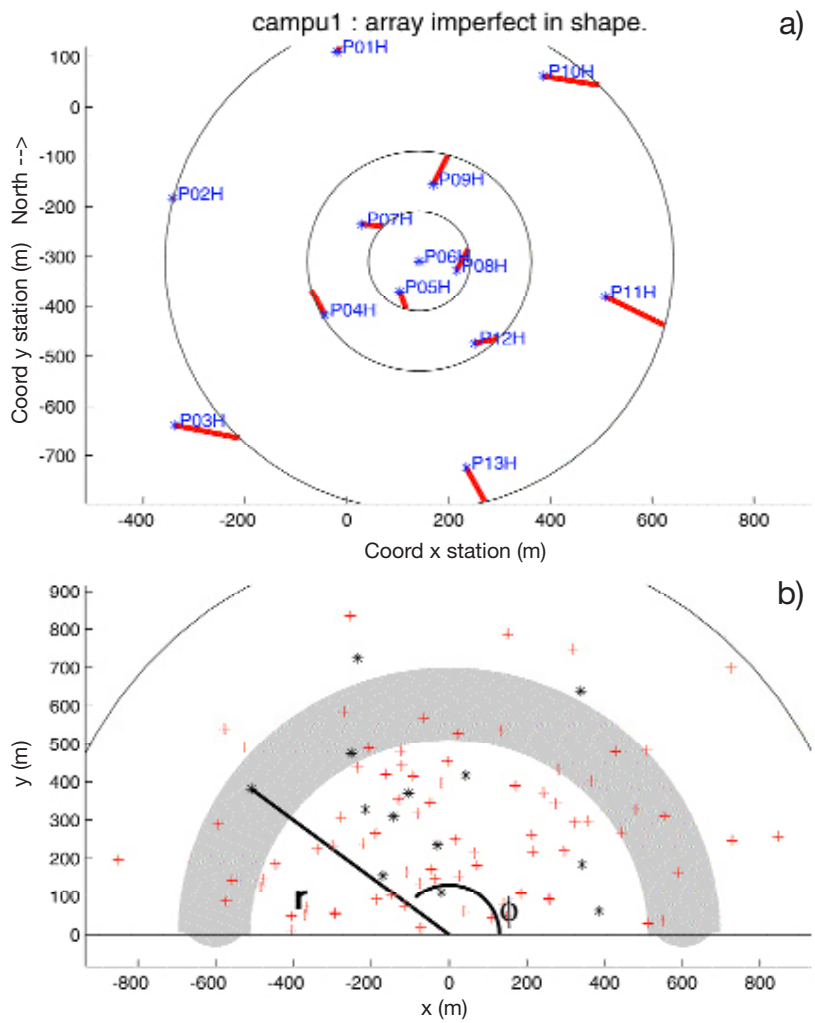

Fig. 3 - **a)** Illustration of the departure of the large "Campus" array from a perfectly regular array (thick strokes represent differences of location from perfect shape). **b)** Distribution in spacing *r* and azimuths φ of all the stations pairs for the large "Campus" array is not uniform (each cross represents a couple of stations of spacing *r* and azimuth φ, stars outline couple with respect to the reference station P06H).

can characterize the structure of the underlying propagation medium. Since the method is based on a statistical investigation in time and space, we assume that the signal is a stochastic noise, stationary in both domains.

3.1. Principle of the method:

Let us first consider the case of a single plane wave propagating along the x direction. The spatial auto-correlation function of the signal $u(x;t)$ for the region $x \in [0, X]$ and the time domain $t \in [0, T]$ is defined as follows :

$$< \phi (\xi, t) >_x = \frac{1}{X} \int_0^X u (x, t)\, u (x + \xi, t)\, dx. \tag{1}$$

From the assumption of signal stationarity both in space and time, it follows that :

$$\phi (\xi) = < \phi (\xi, t) >_x = < \phi (\xi, t) >_t = \frac{1}{T} \int_0^T \upsilon_0 (t)\, \upsilon_\xi (t)\, dt. \tag{2}$$

Where $\upsilon_0 (t) = u (x_0, t)$ and $\upsilon_\xi (t) = u^* (x_0 + \xi, t)$ could be the signals recorded at two stations separated by a distance ξ. In the case of a single dispersive wave, Aki (1957), using the relation between the spectra in time and space, showed that the auto-correlation function can also be expressed like :

$$\phi (\xi) = \frac{1}{\pi} \int_0^\infty \Phi (\omega) \cos \left(\frac{\omega}{c (\omega)}\, \xi \right) d\omega, \tag{3}$$

where $\Phi (\omega)$ is the auto-correlation frequency spectrum, ω is the angular frequency and $c (\omega)$ is the frequency dependent velocity. When the wave is filtered by a narrow-band filter around the frequency ω_0, if $P (\omega_0)$ is the spectral power density and δ the Dirac function, it follows that:

$$\Phi (\omega) = P (\omega_0)\, \delta (\omega - \omega_0). \tag{4}$$

Therefore Eq. (3) becomes:

$$\phi (\xi, \omega_0) = \frac{1}{\pi} P (\omega_0) \cos \left(\frac{\omega_0}{c (\omega_0)}\, \xi \right). \tag{5}$$

and if we define the spatial auto-correlation ratio as $\rho (\xi,\omega_0) = \dfrac{\phi (\xi, \omega_0)}{\phi (0, \omega_0)}$, it follows that:

$$\rho (\xi,\omega_0) = \cos \left(\frac{\omega_0}{c (\omega_0)}\, \xi \right). \tag{6}$$

This relationship may then be inverted in order to obtain the dispersion curve $c\ (\omega_0)$.

When the direction of propagation of the considered wave is not known, Eq. (6) should be expressed in a different way. Let r and φ be respectively the distance and azimuth of the direction between the stations. If θ is the azimuth of propagation, Eq. (6) becomes:

$$\rho\ (r, \varphi, \omega_0) = \cos\left(\frac{\omega_0\, r}{c\ (\omega_0)} \cos\ (\theta - \varphi)\right). \tag{7}$$

This equation indicates that the ratio ρ decreases more rapidly with increasing frequency along the propagation direction ($\varphi = \theta$), and that, in an ideal case, it should be constant along the wave front ($\varphi = \theta \pm \pi/2$). Although the graphical representation of ρ can give an estimation of the direction of propagation (provided simultaneous measurements are available along different azimuths), in general, θ is not known. It is thus necessary to introduce an azimuthal average of the auto-correlation ratio:

$$\overline{\rho}\ (r, \omega_0) = \frac{1}{\pi}\int_0^{\pi} \rho\ (r, \varphi, \omega_0)\ d\varphi.$$

Then, for a wave filtered around ω_0, using Eq. (7), we obtain:

$$\overline{\rho}\ (r, \omega_0) = J_0\left(\frac{\omega_0\, r}{c\ (\omega_0)}\right), \tag{8}$$

where J_0 is the Bessel function of zero order: $J_0\ (x) = 1/\pi \int_0^{\pi} \cos\ (x \cos(\varphi))\ d\varphi$. Therefore, in the case of a Rayleigh wave recorded by vertical components and dropping the index of frequency ω_0 , Eq. (8) gives:

$$\overline{\rho_z}\ (r, \omega) = J_0\left(\frac{\omega\, r}{c_R\,(\omega)}\right), \tag{9}$$

where $c_R\ (\omega)$ is the phase velocity of the dispersive Rayleigh waves. The term $\overline{\rho_z}\ (r, \omega)$ can be obtained by measuring $\rho_z\ (r, \omega, \varphi)$ for several stations located on a semi-circle of radius r with a reference station at the center. Knowing $\overline{\rho_z}\ (r, \omega)$ at different values of the frequency, the phase velocity $c_R\ (\omega)$ can be computed. In order to deal with polarized waves, the spatial auto-correlation ratio $\overline{\rho_r}\ (r, \omega)$ and $\overline{\rho_\varphi}\ (r, \omega)$ shall be computed, in the same way, for the radial and tangential components, respectively. In the general case of a superposition of Rayleigh and Love waves, with parallel and perpendicular polarisation respectively, under the assumption that the contributions of both waves are statistically independent, the auto-correlation ratios are given by (Aki, 1957; Chouet, 1996):

$$\overline{\rho_r}\ (r, \omega) = \alpha\left[J_0\left(\frac{\omega\, r}{c_R\,(\omega)}\right) - J_2\left(\frac{\omega\, r}{c_R\,(\omega)}\right)\right] + (1 - \alpha)\left[J_0\left(\frac{\omega\, r}{c_L\,(\omega)}\right) + J_2\left(\frac{\omega\, r}{c_L\,(\omega)}\right)\right], \tag{10}$$

$$\overline{\rho_\varphi}(r,\omega) = \alpha\left[J_0\left(\frac{\omega r}{c_R(\omega)}\right) + J_2\left(\frac{\omega r}{c_R(\omega)}\right)\right] + (1-\alpha)\left[J_0\left(\frac{\omega r}{c_L(\omega)}\right) - J_2\left(\frac{\omega r}{c_L(\omega)}\right)\right], \qquad (11)$$

where $\alpha(\omega)$ represents the proportion of Rayleigh waves in the wave field energy ($0 < \alpha < 1$). Measuring $\overline{\rho_z}$, $\overline{\rho_r}$, and $\overline{\rho_\varphi}$, and using Eqs. (9), (10) and (11), one can estimate the phase velocities $c_R(\omega)$ and $c_L(\omega)$ and the proportion for each mode.

3.2. Array design and improvements to the SPAC method

The optimal array design for measuring the spatial auto-correlation ratios $\overline{\rho_z}$, $\overline{\rho_r}$, and $\overline{\rho_\varphi}$, is circular in shape. As far as the authors know, in all the previous experiments performed to implement the SPAC method, the arrays were designed in the same way: several stations located on a semi-circle of radius r with one reference station at the center. The accuracy of the azimuthal averaging then depends on the number of stations and their location. The estimated dispersion curves obtained by inversion are relevant only in a narrow frequency band, that depends on the aperture (radius r) of the array and on the sensor characteristics (frequency range and sensitivity). In order to enlarge the validity domain in frequency of the dispersion curves, the experiment is to be repeated with arrays of different radius r.

In case results in the low frequency range are needed, the array must be large enough to be comparable to the wave length of the Rayleigh and Love fundamental modes: this may sometimes lead to apertures larger than 1km. In urban areas, installation of such large aperture arrays is often not easy. Because of the location of buildings, streets and other obstacles, it is no longer possible to have perfectly circular arrays. For instance, in the case of the Grenoble "Campus" site (Fig. 2), the 13 stations that could be installed were located on three imperfectly shaped concentric circles. The exact locations were obtained, in that case, by GPS kinematic measurements. Fig. 3a, shows how the GPS locations differ from theoretical locations (perfectly shaped array). Processing the azimuthal average of the auto-correlation ratio in those conditions did not have much sense, since there were only very few station pairs with identical spacing as depicted on Fig. 3b.

The SPAC method had, therefore, to be modified to account for the variable radius values, as well as for the inhomogenous distribution of azimuths. Inverting the surface wave dispersion curves implicitly assumes a horizontally layered structure, which therefore requires the lateral variation of the sedimentary filling thickness and structure to be small compared to the aperture of the array.

Under this assumption, only relative locations of the station pairs must be taken into account. Thus, from simultaneous recordings of an odd number n of stations around a central reference one, a total of $n(n+1)/2$ correlation values corresponding to all station pairs (spacing r, azimuth φ) may be derived.

Let us consider the array displayed in Fig. 4, consisting of a central "reference" station, and 15 other stations located on a circle of diameter D. When the array has a perfectly regular shape, one can compute $(n+1)/2 = 8$ azimuthally averaged correlations for 8 different values of distan-

ce r_k by: $r_0 = D/2$, and $r_k = D \sin(k\pi/n)$, $(1 \le k \le 7)$. The azimuthal distribution is the same for each radius and corresponds to 15 azimuths (Fig. 4). Square grid or triangular shaped arrays are not well adapted to the method because there are few azimuths available compared to a circular shaped one with the same number of stations.

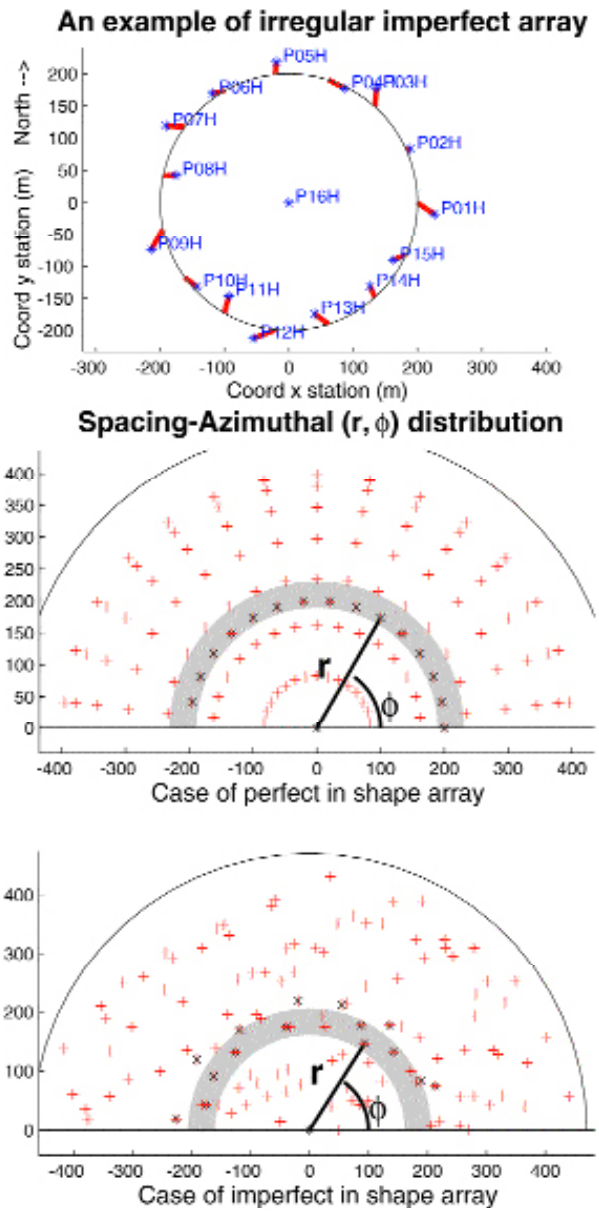

Fig. 4 - **Top:** Example of 16 stations round in shape array (thick strokes represent differences of location from perfect shape). **Middle:** A single 16 stations perfectly round in shape array is equivalent to 8 semi-circular sub-arrays (each cross represents a couple of stations of spacing r and azimuth φ, stars outline couples with respect to the reference station P16H). Thus, one can compute 8 azimuthaly averaged SPAC ratios with only 16 stations (P01H-P16H) recording simultaneously. **Bottom:** In the case of an array imperfect in shape, the calculation of azimuthal averages at constant radius is no longer possible, but the distribution in spacings r and azimuths φ is still pretty uniform. Thus, we compute averaged SPAC ratios on rings $r1$ - $r2$ (grey tint surface) in polar coordinates (r, φ).

Upon installation, the station location has to be adapted to many obstacles that imply an imperfectly shaped array. Fig. 4, also displays an imperfect array and the corresponding (r, φ) distribution with $d_{min} \le r \le D_{max}$. The azimuthal distribution is pretty good, but we can no longer compute azimuthally averaged ratios at a constant radius. Therefore, we have to compute the average of the spatial auto-correlation ratio on rings $(r_1; r_2)$ in the plane (r, φ). From relation (7) it follows that:

$$\begin{aligned}\overline{\rho_{r_1, r_2}}(\omega) &= \frac{2}{\pi (r_2^2 - r_1^2)} \int_0^{\pi}\int_{r_1}^{r_2} \rho(r, \varphi, \omega)\, r\, dr\, d\varphi \\ &= \frac{2}{\pi (r_2^2 - r_1^2)} \int_0^{\pi}\int_{r_1}^{r_2} \cos\left(\frac{\omega r}{c(\omega)} \cos(\theta - \varphi)\right) r\, dr\, d\varphi. \end{aligned} \tag{12}$$

From the properties of definition of the Bessel functions J_0 and J_1 we have:

$$J_0(x) = \frac{1}{\pi}\int_0^{\pi} \cos(x \cos\varphi)\, d\varphi \tag{13}$$

and

$$x\, J_1(x) = \int_0^{x} \mu\, J_0(\mu)\, d\mu. \tag{14}$$

Hence:

$$\begin{aligned}\overline{\rho_{r_1, r_2}}(\omega) &= \frac{2}{r_2^2 - r_1^2} \int_{r_1}^{r_2} r\, J_0\left(\frac{\omega r}{c_R(\omega)}\right) dr \\ &= \frac{2}{r_2^2 - r_1^2} \frac{c(\omega)}{\omega} \left[r\, J_1\left(\frac{\omega}{c(\omega)} r\right)\right]_{r_1}^{r_2}. \end{aligned} \tag{15}$$

Similarly, we could also derive modified relations for horizontal components, corresponding to relations (10) and (11).

Hence, a given array can be divided into several equivalent semicircular sub-arrays k defined by the couples of stations (i,j) the spacing of which r_{ij} verifies $r_{k1} < r_{ij} < r_{k2}$. For each sub-array we calculate the average of the spatial auto-correlation ratio as follows:

$$\overline{\rho_k}(\omega) = \frac{2}{\pi (r_{k2}^2 - r_{k1}^2)} \sum_{r_{k1} < r_{ij} < r_{k2}} \rho(r_{ij}, \varphi_{ij}, \omega)\, \overline{r_k}\, \Delta r_k\, \Delta\varphi_{ij}, \tag{16}$$

with

$$\begin{aligned}\overline{r_k} &= \frac{r_{k2} + r_{k1}}{2}, \\ \Delta r_k &= r_{k2} - r_{k1}, \end{aligned} \tag{17}$$

and

$$\sum_{r_{k1} < r_{ij} < r_{k2}} \Delta\varphi_{ij} = \pi, \tag{18}$$

i.e.

$$\overline{\rho_k}\,(\omega) = \frac{1}{\pi} \sum_{r_{k1} < r_{ij} < r_{k2}} \rho\,(r_{ij}, \varphi_{ij}, \omega)\,\Delta\varphi_{ij}. \tag{19}$$

In the basic case of 5 stations located around a central one, Fig. 5 shows how the averaged auto-correlation ratios $\overline{\rho_k}$ (ω) are computed. The determination of r_{k1} and r_{k2} results from a compromise between the number of stations per ring (azimuthal resolution) and the ratio $\Delta r_k / r_k$ which should be as small as possible. We calculate $\Delta\varphi_{ij}$ as follows: $\Delta\varphi_{ij} = (\varphi_{ij+1} - \varphi_{ij-1})/2$.

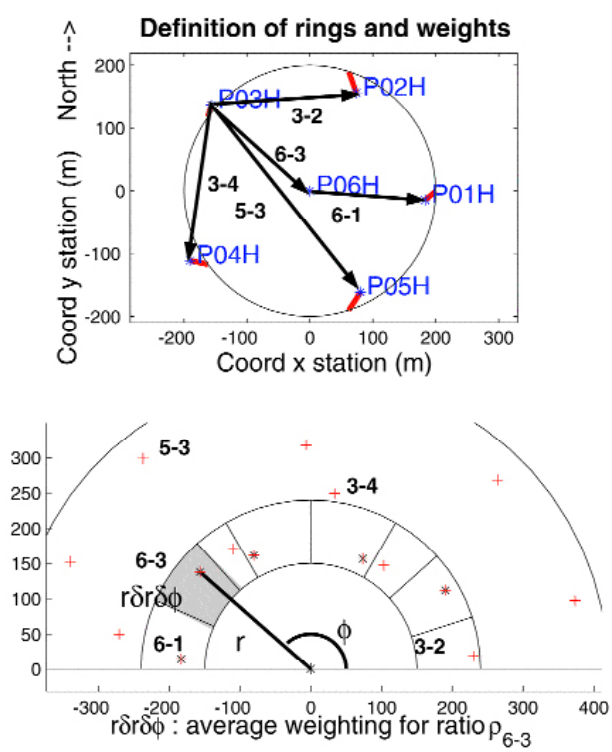

Fig. 5 - In the basic case of a 6 stations array, we describe how are defined rings ($r1$, $r2$) and weights in order to compute the corresponding averaged SPAC ratio, e.g. $r\,\delta r\,\delta\varphi$, the grey shaded element in the weight attributed to the SPAC ratio ρ_{6-3}.

3.3. Inversion algorithm

Once the $\overline{\rho_k}(\omega)$ are obtained, the dispersion curves (i.e. the $c(\omega)$ values) must be computed. This is done through an inversion process. We applied a nonlinear inversion method based on least squares adjustment (Tarantola et al., 1982). The equation can be considered as a nonlinear relation of the form $d = g(p)$, where, d is the data vector (auto-correlation ratios) and p represents the parameter vector ($c_R(\omega)$, $c_L(\omega)$, and $\alpha(\omega)$). The least squares problem is solved by using the iterative algorithm:

$$p_{m+1} = p_0 + C_{p_0p_0} G_m^T (C_{d_0d_0} + C_m C_{p_0p_0} G_m^T)^{-1} [d_0 - g(p_m) + G_m(p_m - p_0)], \tag{20}$$

where m is the iteration index, p_0 represents the a priori parameter vector, $C_{d_0d_0}$ and $C_{p_0p_0}$ are the covariance matrix for data and parameters, respectively, G_m is the partial derivative matrix $G_{ij} = \partial g_i / \partial p_j^{(M)}$, and G_m^T its transpose. For example, in the case of Eq. (15), we have:

$$\frac{\partial \overline{\rho}_{r_1,r_2}}{\partial c_R} = \frac{2}{r_2^2 - r_1^2} \frac{\partial \left(\frac{c_R}{\omega} \left[r J_1\left(\frac{\omega}{c_R} r\right) \right]_{r_1}^{r_2} \right)}{\partial c_R} = \left[\frac{\omega r^3}{c_R^2} J_2\left(\frac{\omega}{c_R} r\right) \right]_{r_1}^{r_2}. \tag{21}$$

The prameters c_R and c_L are defined as continuous functions of angular frequency ω. The corresponding components of the parameter covariance matrix are given by Tarantola et al. (1982):

$$C_{p_0p_0}(\omega, \omega') = \sigma^2 \exp\left[-\frac{1}{2} \frac{(\omega, \omega')^2}{\Omega^2} \right], \tag{22}$$

where σ is the standard deviation of parameter p, and Ω is a correlation length in the domain of the angular frequencies, which controls the smoothness of the solution. Estimations of the errors on the parameters are obtained from the a posteriori covariance matrix:

$$C_{pp} = C_{p_0p_0} - C_{p_0p_0} G^T (C_{d_0d_0} + GC_{p_0p_0} G^T)^{-1} GC_{p_0p_0}$$

3.4. Tests of the SPAC method

Before applying this modified SPAC method to an analysis of the Grenoble basin data, we performed a few preliminary tests. The first and most simple one consists in simulating the propagation of a seismic noise signal through an array as a non-dispersive plane wave (phase velocity: 400 m/s).

With this objective in mind, we selected a real microtremor recording obtained during the Grenoble experiment, and derived a fictitious set of array recordings by simply modifying its phase for each station of the array displayed in Fig. 4, according to the station location and

the assumed phase velocity and propagaton direction. Metaxian (1997) recommended using a minimum of 7 station pairs to have a reliable azimuthal average. In our case, to be on the safe side, we decided to derive the azimuthal average from at least 13 station pairs per ring. The inversion process is applied simultaneously to seven different semi-circular sub-arrays (k = 1 to 7). The corresponding distance intervals ($dmin_k$; $dmax_k$) are detailed in Table 1.

Fig. 6, shows that the computed SPAC averaged ratios (solid black lines) fit the corresponding Bessel functions (grey dashed lines), i.e.

$$\overline{\overline{\rho}}_{dmax_k,\, dmin_k}(\omega) = \frac{800}{\omega\,(dmax_k^2 - dmin_k^2)}\left[r\, J_1\left(\frac{\omega}{400}\,\frac{dmax_k}{dmin_k}\, r\right)\right] \quad , \tag{23}$$

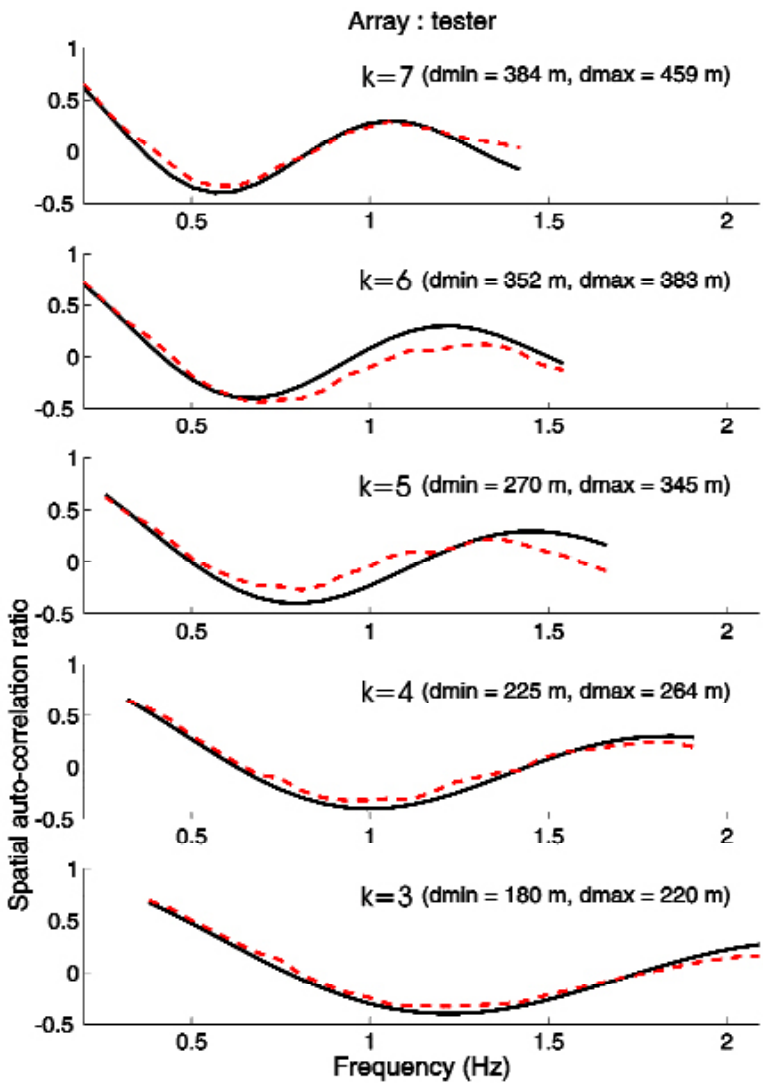

Fig. 6 - Averaged SPAC curves for the vertical component of a real seismic noise signal propagated by calculation (non-dispersive plane wave assumption) through the imperfect round in shape array defined in Fig. 4 (dashed lines), compared with corresponding theoretical first-order Bessel function (solid lines). The averaged SPAC ratios were calculated on 7 rings of different spacing ranges (*dmin*, *dmax*), but only 5 are shown here (k = 3 to 7).

pretty well even in the case of imperfectly shaped array (only five curves are displayed). It supports the relevance of relation (15) that allows us to enlarge the application domain of the SPAC method without introducing noticeable errors.

Fig. 7 displays the dispersion curve we inverted using the algorithm briefly described in part C: it presents a very satisfactory fit with the value of 400 m/s we have arbitrary chosen as constant propagation velocity. We observe however, that it does not fit either under 0.3 Hz or over 2.5 Hz.

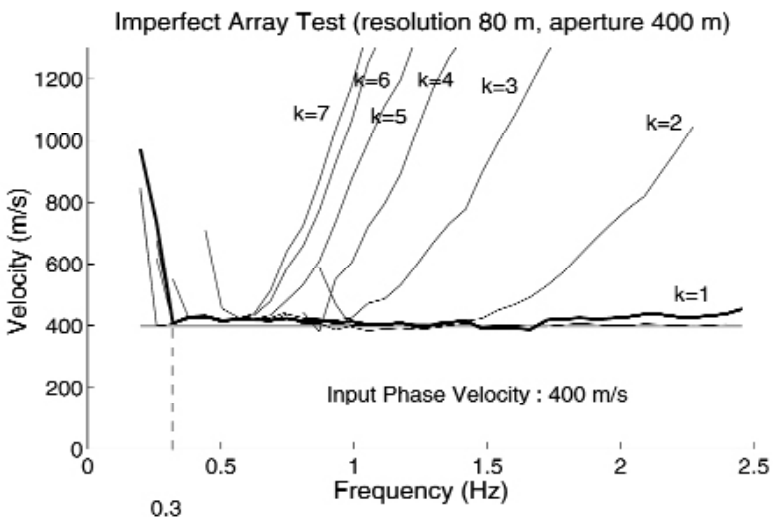

Fig. 7 - Dispersion curve obtained by inversion (thick black line) from all averaged SPAC ratios previously computed compared with the input propagation velocity of 400 m/s (thick grey line). This result fits relatively well for frequencies f > 0.3 Hz. Thin black lines curves are obtained separately by inversion from the averaged SPAC ratio for each single ring (k = 1 to 7).

The width of the frequency validity domain of the result is correlated to the resolution and aperture of the array. If we process data of each single ring separately, we observe that the dispersion curves obtained fit the value of 400 m/s only in narrow frequency domains correlated to the station pairs spacings. Table 1 shows the corresponding frequency band inside which the method is relevant for each value of station pairs spacing.

Table 1 - Sub–arrays of the test's array : station pairs spacing and the corresponding frequency band (constant phase velocity: 400 m/s).

Ring number	**Spacing range** d_{min} - d_{max} (m)	**Frequency band** f_{min} - f_{max} (Hz)
1	73- 98	1.0 -2.5
2	112-172	0.6 -1.5
3	180-220	0.4 -1.0
4	225-264	0.3 -0.9
5	270-345	0.3 -0.7
6	352-383	0.3 -0.65
7	384-459	0.25-0.65

The constant velocity assumption is, however, very far from reality, as we are interested in surface waves. We, therefore, decided to simulate the propagation of dispersive plane waves through a perfectly circular array. The Rayleigh waves dispersion curve chosen as input corresponds to a onedimensional model with a linear velocity gradient of 1.4 s^{-1} for both P and S waves in sediments down to a bedrock depth of 700 m. The corresponding auto-correlation ratios shown on Fig. 8 still compare very well with the theoretical first order Bessel function. And, as in the previous case, the dispersion curve we computed using the SPAC method (vertical component analysis) fits the input dispersion curve down to 0.4 Hz (see Fig. 9) relatively well.

These results, though partial, are nevertheless very encouraging for the relevancy of the SPAC technique, to retrieve the Rayleigh dispersion curves, at least for 1D structures, and in

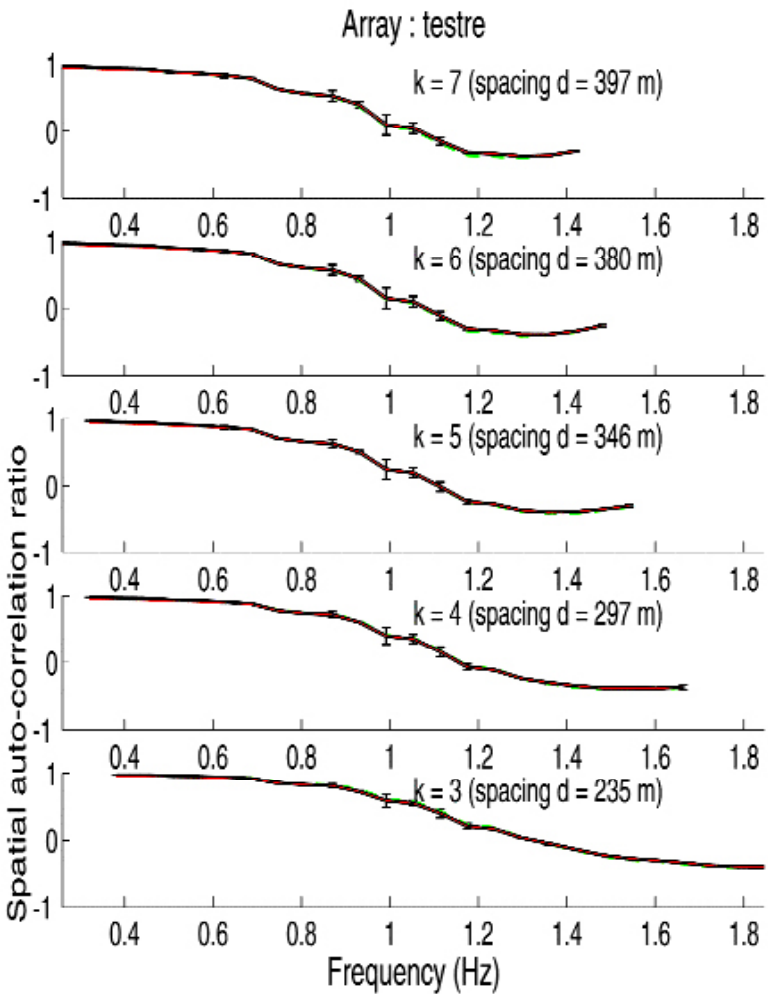

Fig. 8 - Averaged SPAC curves for the vertical component of a real seismic noise signal propagated by calculation (dispersive plane wave assumption) through the perfectly circular array defined in Fig. 4 (dashed lines), compared with the corresponding theoretical first-order Bessel function (solid lines). The averaged SPAC values were calculated on 7 semi-circular sub arrays station pairs of different spacing d, but only 5 are shown here (k = 3 to 7).

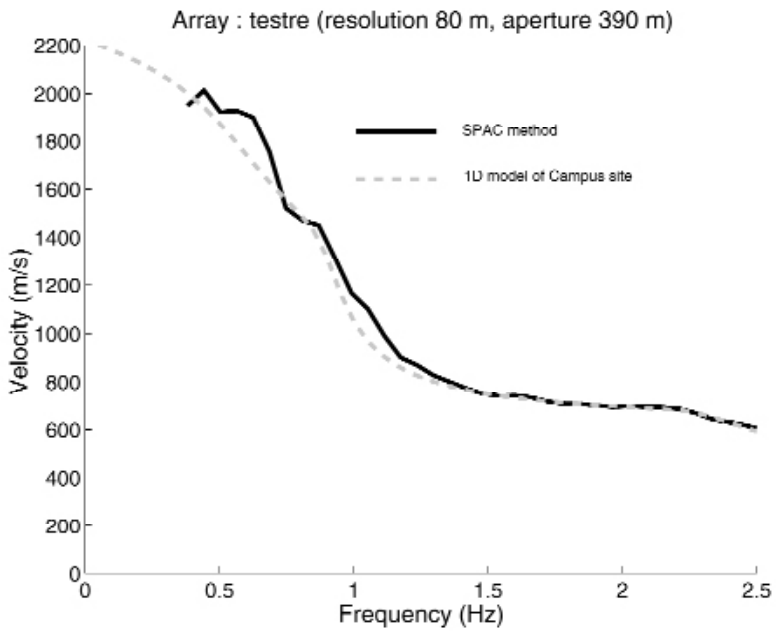

Fig. 9 - Dispersion curve obtained by inversion (thick black line) from all averaged SPAC curves previously computed compared with the input Rayleigh wave dispersion curve (thick grey dashed line), of 400 m/s (thick grey line). This result fits relatively well for frequencies f > 0.4 Hz. Thin black lines curves are obtained separately by inversion from the averaged SPAC ratio for each single ring (k = 1 to 7).

the case the assumption of predominant fundamental modes is valid. However, before using the modified SPAC method as a routine investigation technique, many more specific tests have certainly to be performed, in order to better assess and quantify its robustness. We will simply indicate here some of the issues that should be addressed: non-stationary spectral contents of noise (including transients), local noise sources located inside the array, sensitivity to contamination of the wavefield by overtones, large lateral variations in layer thicknesses or velocities. Comprehensive investigations on these issues would however require at least a whole PhD work, and would largely exceed the scope of the present paper, simply intended to present the improvements to the SPAC technique, and two example applications.

4. Processing of the Grenoble experimentation data

The modified SPAC technique was thus used to derive the dispersion curve of Rayleigh waves for each site of the Grenoble 99 experiment. Here we will only present the results from 2 sites, “Campus” and “Bon Pasteur”, which correspond to the two largest arrays, and therefore allow us to obtain results at low frequencies. Both sites are displayed on the map in Fig. 1. Only vertical data have been considered so far, but horizontal components may be processed in the same way too.

4.1. Computing the SPAC averaged ratios

The first step is to compute averaged spatial auto-correlation ratios for several rings and for subsequent time windows. Here we selected 100 time windows of 8192 points width each (i.e. 65.5 s). Fig. 10 displays the azimuthally averaged ratios computed from Campus site data (thick black lines). These ratios look like Bessel functions, as expected. Each curve corresponds to the mean ratio derived from all of the 100 time windows. The vertical bars correspond to the standard deviation of the auto-correlation ratios obtained from these 100 different time windows. They are very small, and strongly support the assumption of stationarity in time.

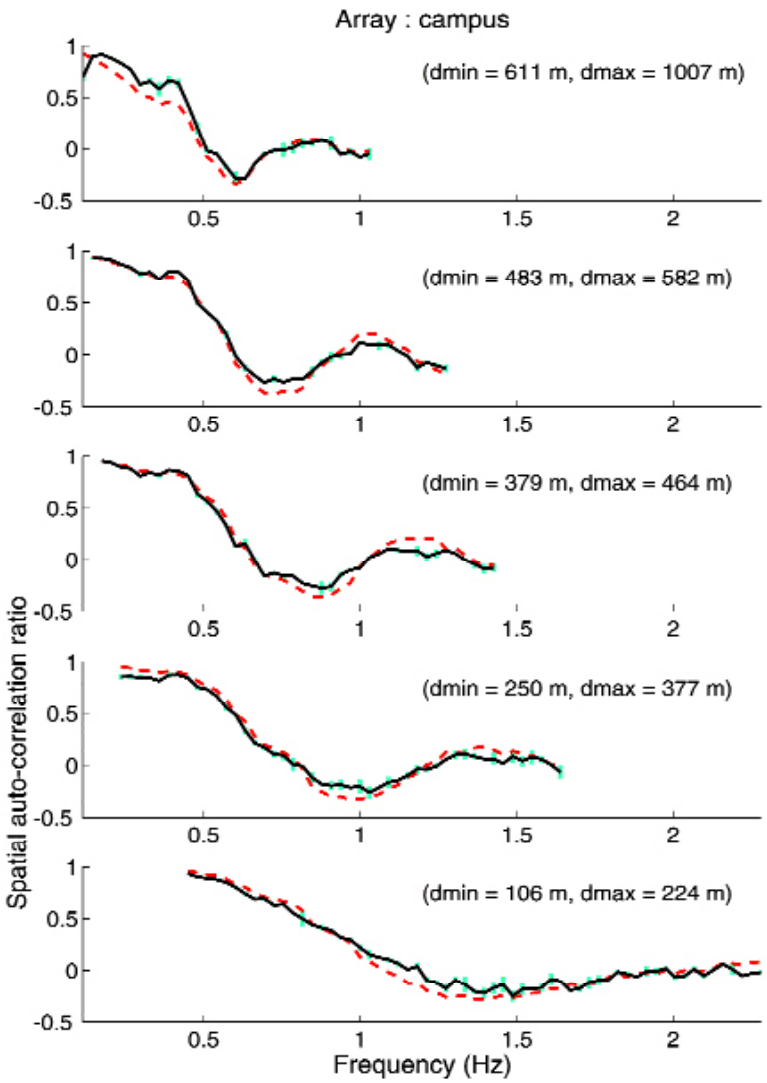

Fig. 10 - Averaged SPAC curves for the vertical component of the Campus measurements (thick lines). Dashed curves, which correspond to the global inversion result, must fit all values (for each ring) at the same time. Vertical thick grey strokes indicate standard deviation for all frequencies (correlation values are computed on several time windows).

4.2. Inversion to derive the Rayleigh dispersion curve

In Fig. 10, dashed lines correspond to the theoretical correlation curves when velocity values are inverted from all observed correlation curves. They fit the averaged ratio curves pretty well. The dispersion curve of Rayleigh waves we obtain, shown in Fig. 11 (thick solid line), is the lower envelope of all the curves inverted ring by ring (thin solid lines and dashed lines on top of Fig. 11). We also computed the dispersion curves for large and small "Campus" arrays separately (see bottom of Fig. 11). Those curves merge together around 1.2-1.3 Hz. Limitations due to array size appear clearly. The frequency band inside which the result seems to be relevant is 0.4-1.5 Hz in the case of the large array (1 km of aperture) and 1-5 Hz for the small array (120 m of aperture).

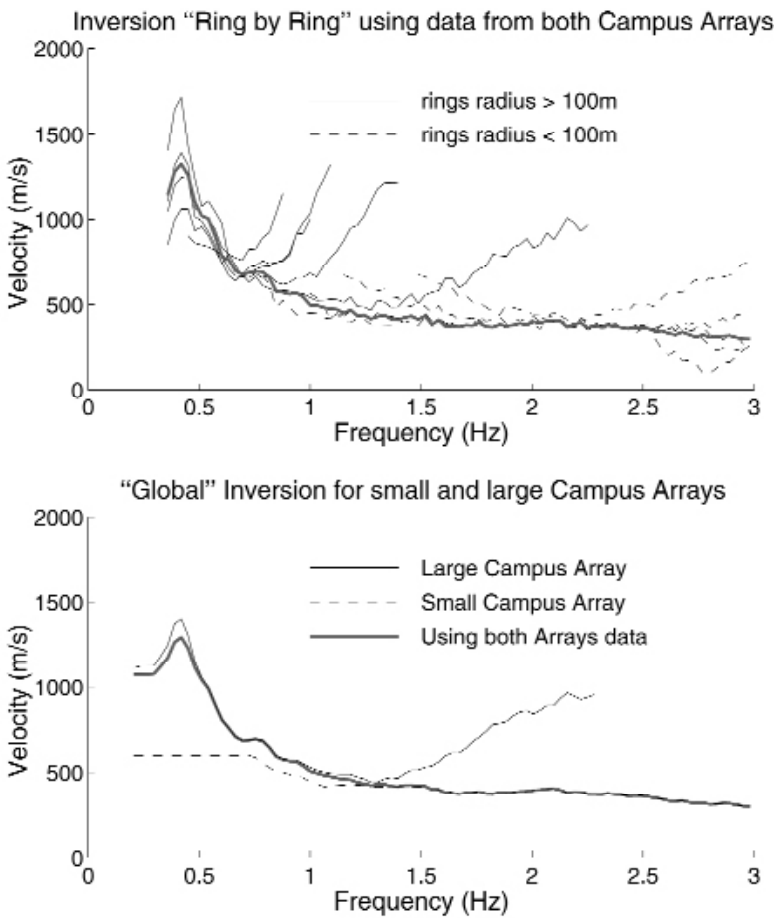

Fig. 11 - Derived dispersion curves of Rayleigh fundamental mode. Thick line is obtained by global inversion (taking all averaged correlation values into account). **Top:** Each thin line (solid for large array data, dashed for small array data) represents the result obtained by inversion of the averaged ratio corresponding to an individual ring. The accurate frequency band for an individual ring of station pairs is very narrow (see Table 2). **Bottom:** Dispersion curves obtained computing large Campus array data (upper thin line), small Campus array data (lower thin dashed line) and both arrays data (thick solid line). If we want to compute dispersion curves for a large frequency band, we have to repeat measurements with different array sizes.

4.3. Limitations due to array shape and size

We checked if the method was still relevant for this kind of array shape. As for the previous tests, we used a real seismic noise signal for which we modified the phase to simulate its propagation through the array at a non-dispersive velocity. We obtained a pretty good confidence in the frequency band 0.2-1.8 Hz for the large "Campus" array (aperture 1 km) as it is shown on Fig. 12 (constant phase velocity of 500 m/s). This frequency band becomes narrower if we process only ratio values for one single ring (thin lines), particulary for larger rings that we know to have a bad azimuthal distribution in the case of the Grenoble experiment.

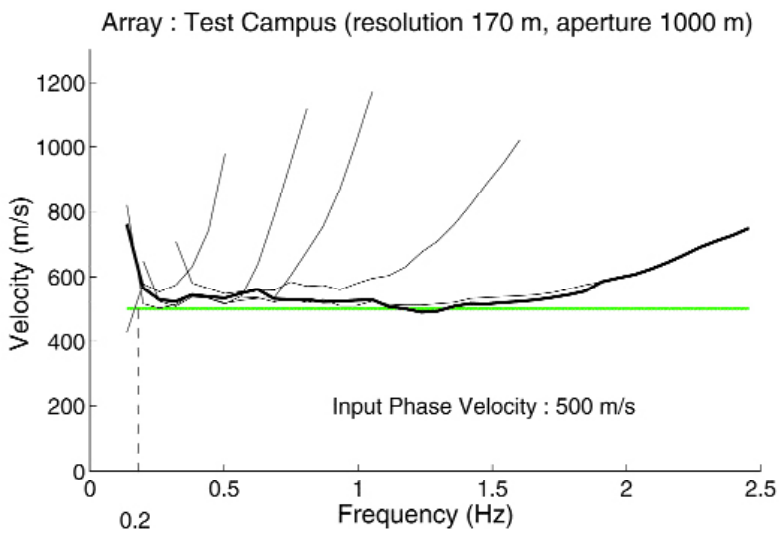

Fig. 12 - Example of test performed in order to study the limitations due to the shape and size of the large Campus array. Data of each sub-array ring have been processed (thin solid lines). The thick black line corresponds to the global inversion result. It is the downwards envelope of all the thin solid lines.

We also observed that the dispersion curve obtained by inversion of all averaged ratios, is at the same time, the downward envelope's curve of all those that are computed for one single ring. For the small Campus array (aperture 120 m), we observe a good confidence of the result in the frequency band 1-5 Hz. Table 2 summarizes the tests performed in order to relate aperture, resolution and azimuthal distribution with the expected confidence frequency band.

Table 2 - Sub-arrays of the Campus arrays: relation between station pairs spacing and wavelength.

Spacing range r_1 - r_2 (m)	**Frequency band** f_{min} - f_{max} (Hz)	**Phase velocity** $c(\omega)$ (m/s)	**Wave length** λ (m)
100- 220	0.6 -0.95	500- 800	500-1300
250- 370	0.4 -0.8	550- 900	700-2200
400- 500	0.3 -0.7	650-1100	800-3700
500- 600	0.25-0.6	800-1300	1300-5200
600-1000	0.2 -0.5	1050-1600	2600-8000

The limitations due to sensor response are related to the phase delays caused by differences in eigenfrequencies of seismometers. Scherbaum et al. (1999) showed that this effect cannot be neglected for lower frequencies ($f < 0.4$ Hz). This may explain the difference between tests and real data processing for low frequencies.

4.4. Results for Campus and Bon Pasteur sites

The results obtained for the two sites "Campus" and "Bon Pasteur" are displayed in Figs. 13 (dispersion curves) and 14 (inverted velocity profiles), which also provide a comparison with

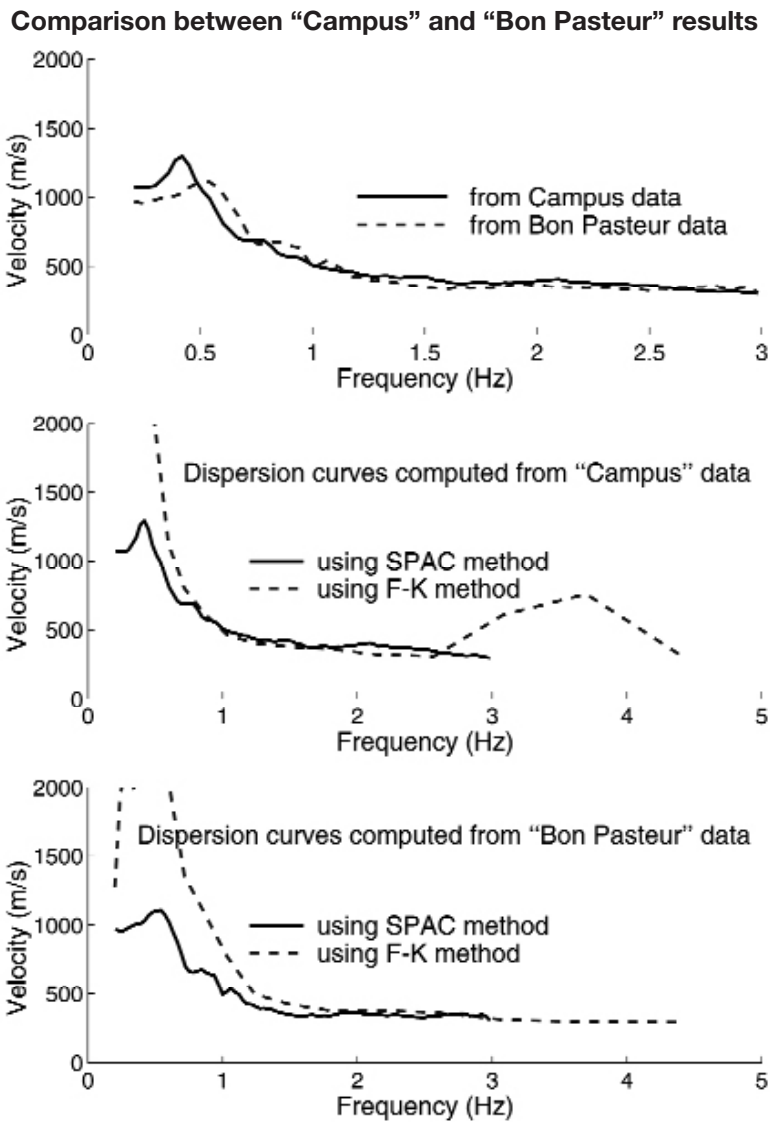

Fig. 13 - Comparison between Rayleigh fundamental mode dispersion curves derived from "Campus" and "Bon Pasteur" data using two methods: SPAC modified method and a semblance based frequency-wavenumber (*f-k*) analysis (Scherbaum et al., 1999).

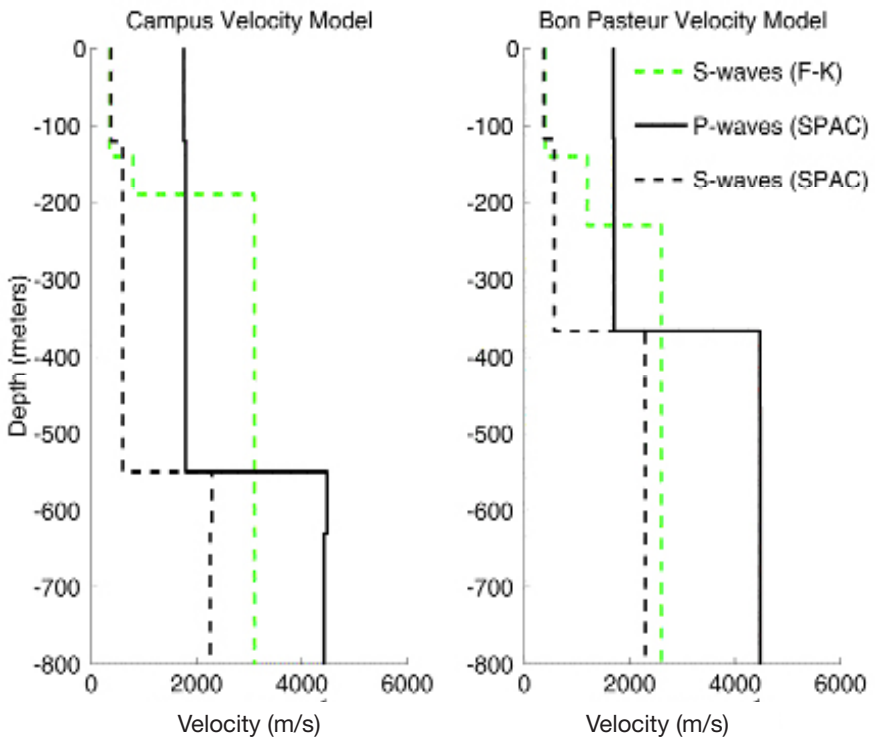

Fig. 14 - Comparison between velocity models obtained from Campus and Bon Pasteur data using *f-k* analysis (grey dashed line) and modified SPAC method (thick and dashed black lines).

previous estimates obtained with the semblance-based, *f-k* method (Scherbaum et al., 1999). According to Fig. 1, the sediment thickness should be larger at Campus (around 700 m) than at Bon Pasteur (600 m). One must notice, however, that, for both sites, it does exhibit significant variations over the array dimensions (of about 300 m at Bon Pasteur, and 200 m at Campus).

Fig. 13 calls for essentially two comments:

1. Campus and Bon Pasteur SPAC dispersion curves are very similar, but nevertheless exhibit some slight differences at low frequencies: in between 0.5 and 0.7 Hz, phase velocities are higher for Bon Pasteur than for Campus (while this trend is reversed below 0.5 Hz). Beyond 1 Hz however, the two curves are almost similar;
2. a larger, systematic difference is observed at both sites between the *f-k* and SPAC estimates: the former yield much higher low frequency phase velocities.

The curves have then been used to invert the velocity profile, using Herrmann's software (Herrmann, 1987). Here we are showing here only preliminary results, using a very simple, 3- layer profile, in which we did not take into account the existence of a velocity gradient. The slight velocity differences result in significant changes in velocity profiles.

The sediment thickness values estimated at Bon Pasteur and Campus from SPAC results are, respectively, 370 m and 550 m. These values are significantly less than the estimations displayed on Fig. 1. This misfit may have at least two origins:

a) the thickness variations underneath the arrays do significantly perturbate the dispersion curves, so that the laterally unvarying 1D assumption is too strong and affects the results

(one may imagine that the lateral variations will broaden the bandwidth of the dispersion curve fall off, but this definitely needs to be looked at carefully);

b) the "homogeneous layer" hypothesis assumed for the inversion is also too strong, and biases the thickness estimates when there actually exists a large velocity gradient. However, it is rather satisfactory to obtain a larger thickness at Campus than at Bon Pasteur.

The S-wave velocity estimates derived from SPAC results (570 to 600 m/s, see Table 3) are very consistent with the average S-wave velocity values measured in the Montbonnot borehole. Also interesting - though less well constrained - is the estimate of S-wave velocity in bedrock (2260 to 2300 m/s) which is consistent with the geology (Bajocian limestone / shale).

The thicknesses derived from the *f-k* curves are much lower (by a factor of 2.5 to 3) than those derived from the SPAC curves. Given the other geophysical information available in the area, we are entitled to assign more credit to the SPAC technique. As discussed previously, this large discrepancy may be due to phase inaccuracy at low frequency for Le3D enlarged sensors. This "preference" for the SPAC technique, however, cannot be generalized: it needs many other comparisons at other sites and other frequency bands.

Table 3 - S–waves Velocity profiles for both Campus and Bon Pasteur sites. (FK: frequency wavenumber analysis; LT: layer thickness (m); Vs: S–wave velocity (m/s)).

	Campus				**Bon Pasteur**			
	FK		SPAC		FK		SPAC	
	LT	Vs	LT	Vs	LT	Vs	LT	Vs
1	140.	350.	120.	376.	140.	400.	117.	376.
2	50.	800.	430.	601.	90.	1200.	250.	571.
3	100.	3100.	80.	2292.	100.	2600.	100.	2292.
Halfspace	0.	3100.	0.	2260.	0.	2600.	0.	2300.

5. Conclusion and perspectives

This work - though still to be considered as preliminary - leads to several important conclusions. It first confirms the possibility of deriving dispersion curves of surface waves from array measurements of background seismic noise, even at low frequencies and for very thick sediments (i.e., several hundred meters). It thus offers an interesting alternative to the SASW technique with active sources, which cannot generally offer penetration depths larger than 30 to 50 m.

The SPAC technique seems to be more easily applicable to low frequencies than the *f-k* technique.

In addition, its initial formulation for circular arrays has been extended to arbitrary shapes, provided it offers a good distribution as to the inter-station azimuthal and spacing coverage. This extension/improvement is particularly important in urban areas where the building environment makes it impossible to install regular circular arrays, especially when a large aperture is needed. Finally, the SPAC technique also presents the advantage of outlining very clearly the limitations linked to array size.

For the specific Grenoble case, the results obtained with the modified SPAC technique are qualtitatively and quantitatively consistent with the available geophysical information. It confirms both the large thickness values and the corresponding average S-wave velocity values. Comparing the cost of such measurements, with those of other geophysical techniques (borehole logging, seismic profiling), we recommend the use of this technique for site response microzoning studies in areas covered with thick quaternary deposits, at least as a preliminary investigation tool.

There remain, however, a number of issues that require further investigations. Of particular importance for alpine valleys is the relevance of 1D dispersion curves for structures presenting large lateral variations (2D or 3D), as well as the need to improve the velocity profile inversion process from dispersion curves, in order to take into account velocity gradients, and to obtain estimates of the error bars on velocity values. Another important work direction is the use of horizontal components: the present work only used vertical components, and its reliability at very low frequencies is greatly impaired by lack of energy - especially in sites away from oceans. As the low frequency content on the horizontal component is generally shifted to lower frequencies (as shown by the H/V curves), one may hope to extend the dispersion curve down to lower frequencies (0.2 Hz here), which would greatly improve the reliability of the profile inversion.

These important issues will be investigated in the coming years by a consortium of European teams, within the framework of the EC funded project named "SESAME" (grant EVG1-CT-2000-00026).

Acknowledgments. This work was made possible through the funding of several agencies: the PGRN ("Pole Grenoblois sur les Risques Naturels"), the National Program on Natural Hazards (PNRN) of INSU-CNRS, and the IPSN (Institute of Nuclear Protection and Safety). We are also grateful to the thorough reading and constructive comments of two anonymous reviewers.

References

Aki K.; 1957: *Space and time spectra of stationary stochastic waves, with special reference to microtremors*. Bull. Earthq. Res. Inst. Tokyo, **35**, 415-457.

Chouet B.; 1996: *New methods and future trends in seismological volcano monitoring*. In: Scarpa R. and Tilling R.-I. (eds), Monitoring and Mitigation of Volcano Hazards, Springer-Verlag, Berlin, pp. 23-97.

Cornou C.; 2002: *Traitement d'antenne et imagerie sismique dans l'agglomeration grenoblaise. Implications pour le risque sismique*. Thèse de Doctorat de l'Universite Joseph Fourier, Grenoble.

Cotton F., Berge C. and Lemeille F.; 1998: *Three-dimensional simulation of earthquakes in Grenoble's Basin*. In: Irikura K., Kudo K., Okada H. and Sasatami T. (eds), The Effects of Surface Geology on Seismic Motion, A.A. Balkema, pp. 873-879.

Dietrich M., Bordes C., Bard P.-Y. and Lemeille F.; 2001: *Géophysical exploration for site effects assesment: borehole measurements and vibroseis profiling in the Isère valley near Grenoble, France*. EGS, communication, SE12.04.

Gignoux M.; 1944: *L'epaisseur des depots quaternaires dans la plaine de Grenoble*. CR de la Soc. Geol. de France, **8**, 77.

Herrmann R.B.; 1987: *Computer programs in seismology Vol. 4*, St Louis Univ., St Louis, Mo.

Lebrun B.; 1997: *Les effets de site: Etude experimentale et simulation de trois configurations*, Thèse de doctorat, Universite Joseph Fourier, Grenoble, 194 pp.

Metaxian J.P. and Lesage P.; 1997: *Permanent tremor of Masaya Volcano, Nicaragua: wave field analysis and source location*. J. Geoph. Res., **102**, 22529-22545.

Scherbaum F., Riepl J., Bettig B., Ohrnberger M., Cotton F. and Bard P.Y.; 1999: *Dense array measurements of ambient vibrations in the Grenoble basin to study local site effects*, AGU.

Tarantola A. and Valette B.; 1892: *Generalized nonlinear inverse solved using the least squares criterion*. Rev. Geophys., **20**, 219-232.

Vallon M.; 1999: *Estimation de l'épaisseur d'alluvions et sédiments quaternaires dans la région grenobloise par inversion des anomalies gravimétriques*. In: IPSN/CNRS Internal Report, 34 pp.